Inorganica Chimica Acta, 20 (1976) 243–250

X-Ray Diffraction Study of Fe(III)-Exchanged X-Type Zeolite

N. P. EVMERIDES, B. BEAGLEY and J. DWYER

University of Manchester Institute of Science and Technology, P. O. Box 88, Sackville Street, Manchester M60 1QD, U.K.

(Received May 26, 1976)

Three alternative models are proposed to explain the map obtained from a difference Fourier synthesis for a NaFeX zeolite (30% exchanged). The models are based on the extent of distortion of the zeolitic structure which arises when sodium ions are replaced by ferric ions.

Introduction

Metal ion exchanged synthetic zeolites have provided the basis for extensive research in recent years due to their capacity to operate as catalysts, drying agents, sieving agents *etc.* [1–10].

Transition metal ion exchanged zeolites are currently being investigated in redox reactions to assess their oxidative catalytic activity.

Fe(III) exchanged (A, X) zeolites are regarded as potential agents for selective oxidation [11–14].

Various investigators have pointed out the instability of (A, X) zeolitic structures when Fe(III) ions are exchanged for Na(I) [15–18].

The X-ray diffraction technique has recently been used to assess the crystallographic sites of the metal ions in the zeolitic structure of partially and totally exchanged zeolites by using usual difference Fourier syntheses and least squares procedures from intensity data obtained from powder techniques [19–23] or single crystal techniques [24–26].

Method

The starting material NaX (powder) was exchanged with $Fe(SCN)_3$ solution to obtain the FeNaX sample.

Due to the instability of the zeolitic structure to Fe(III) ions at higher levels of Fe(III) ion exchange, special care was taken by correct choice of conditions to limit the exchange and minimise structure breakdown.

Chemical analysis of the FeNaX sample showed 30% exchanged Fe(III) for Na(I) and surface area measurements of the sample showed only an 8% loss of microporosity.

The sample FeNaX and a reference sample of NaX were brought to the same hydration level by leaving them for several days in the air after a moderate evacuation at 60 °C for five hours.

X-ray powder diffraction patterns were taken at room temperature by using a Phillips diffractometer.

Line intensities up to a 2θ value of 100° were estimated by planimeter for both samples (FeNaX, NaX).

The structure factors of NaX, F_{lit} (hkl), obtained by Olson [25] in his single crystal study, were used to generate hypothetical powder line intensities, $I_{lit}(N)$, for NaX (*n.b.* $N = h^2 + k^2 + l^2$, because of the cubic symmetry). In deriving $I_{lit}(N)$, account was taken of the complication that many powder lines do not have unique indices, hkl. Thus, for a line having two components, for example,

$$I_{lit}(N) = I_{lit}(hkl) + I_{lit}(h'k'l') = aF^2_{lit}(hkl) + bF^2_{lit}(h'k'l') \quad (1)$$

where a and b are the appropriate constants incorporating Lorentz, polarization and multiplicity factors. The powder line intensities $I_{Na}(N)$ and $I_{Fe}(N)$, for the present samples of NaX and FeNaX were normalized to $I_{lit}(N)$.

Each of the normalized $I_{Fe}(N)$ was split into its components, *e.g.* $F_{fe}(hkl)$ and $F_{Fe}(h'k'l')$, as follows. As for the literature example above,

$$I_{Fe}(N) = I_{Fe}(hkl) + I_{Fe}(h'k'l'), = aF^2_{Fe}(hkl) + bF^2_{Fe}(h'k'l) \quad (2)$$

Hence, by means of the assumption

$$F^2_{Fe}(h'k'l')/F^2_{Fe}(hkl) = F^2_{lit}(h'k'l')/F^2_{lit}(hkl) = c \quad (3)$$

we have

$$F^2_{Fe}(hkl) = I_{Fe}(N)/(a + bc). \quad (4)$$

When the square root is taken, and given the same sign as $F_{lit}(hkl)$, the $F_{Fe}(hkl)$ is obtained. The other component has $F_{Fe}(h'k'l') = c^{1/2}F_{Fe}(hkl)$ with the appropriate sign. Lines with any number of components can be treated in a similar way, and the same treatment may be applied to obtain the structure factors $F_{Na}(hkl)$. The structure factors so obtained for NaX and FeNaX were further normalized to Olson's structure factors for NaX.

The Fourier transform of $F_{Na}(hkl) - F_{Fe}(hkl)$ was computed giving a difference electron density map. Three runs using a different number of planes (535, 450, or 147) in each run were made. The run

TABLE I. Literature Atomic Positions for Na13X.[a]

Atom	Wyckoff Position	Occupancy	No/Unit Cell	Fractional Co-ordinates		
				X	Y	Z
T_1	g	1.00	96.0	−0.05291	0.12457	0.03509
T_2	g	1.00	96.0	−0.05352	0.03671	0.12309
O_1	g	1.00	96.0	−0.1099	0.0002	0.1054
O_2	g	1.00	96.0	−0.0025	−0.0041	0.1445
O_3	g	1.00	96.0	−0.0321	0.0730	0.068
O_4	g	1.00	96.0	−0.0706	0.0772	0.1761
Na1	c	0.56	9.0	0.0	0.0	0.0
Na2	e	0.25	8.0	0.060	0.060	0.060
Na3A	e	0.38	12.2	0.230	0.230	0.230
Na3B	e	0.37	11.8	0.238	0.238	0.238
OW_1	e	0.36	11.5	0.074	0.074	0.074
OW_2	g	0.27	25.9	0.093	0.086	0.176
OW_3	e	0.25	8.0	0.245	0.245	0.245
OW_4	g	0.13	12.5	0.281	0.298	0.275
OW_5	g	0.31	29.8	0.353	0.345	0.186
OW_6	g	0.29	27.8	0.239	0.240	0.392
OW_7	g	0.18	17.3	0.174	0.204	0.422
OW_8	g	0.17	16.3	0.212	0.387	0.288
OW_9	g	0.10	9.6	0.312	0.381	0.200
OW_{10}	g	0.14	13.4	0.258	0.412	0.204

[a] Data adapted from Olson [25] for space group Fd3 and origin at 3.

TABLE II. Negative Peaks from Difference Fourier Analysis.

Peak Designation	Fractional Co-ordinates			Model 1	Model 2	Model 3	Nearest Na13X Element	Peak Height[a]
	X	Y	Z					
1	0.000	−0.0004	0.180		O_2	Si	O_2	H
2	0.208	0.308	0.433	Fe	Fe	Fe	OW_7	H
3	−0.051	0.125	0.125	Fe	Fe	Si	O_2 or O_4	H
4	0.050	0.050	0.050	Fe	Fe	Fe	I′	H
7	0.200	0.200	0.241	Fe		O_2	II	H
7′	0.183	0.233	0.217		O_2		II	V.L.
109	−0.058	0.033	0.017	Fe	Fe	Fe	I	H
9	0.233	0.316	0.258	H_2O	O_4	H_2O	OW_3	H
10	−0.058	0.042	0.200			Si	O_4	H
11	−0.108	0.0504	0.183	H_2O	H_2O	H_2O	O_4	V.L.
13	0.171	0.287	0.388	H_2O	H_2O	H_2O	OW_8	M
14	0.004	−0.058	0.250	Fe	O_4	O_1	O_2 or O_1	H
16	0.008	0.058	0.304	Fe	O_2	O_4	O_4 or O_1	H
18	−0.116	0.050	0.075		O_1	O_1	O_1	M
20	0.0	0.0	0.125		O_2	O_2	O_2	M
21	0.112	0.0	0.150	H_2O	H_2O	O_3	OW_2	L
22	0.267	0.316	0.242	H2O	O_4	H_2O	OW_3	V.L.
23	0.375	0.375	0.462	H_2O	H_2O	H_2O		M
26	0.350	0.325	0.200	H_2O	H_2O	H_2O	OW_9	M
29	0.246	0.362	0.250	H_2O		Al	OW_8	V.L.
31	0.358	0.467	0.183	H_2O	H_2O	H_2O	OW_9 or OW_{10}	M
33	−0.0496	0.108	0.175			O_4	O_4	H
100	0.083	0.042	0.175	H_2O		H_2O	OW_2	M
105	0.750	0.042	0.108	H_2O	H_2O	H_2O	OW_1	M
111	−0.087	0.004	0.051			Al	O_1	M
114	−0.046	0.050	0.288				O_2 or O_1	V.L.
121	0.296	0.296	0.496	H_2O	H_2O	H_2O		M
122	0.192	0.275	0.483	H_2O	H_2O	H_2O	OW_6	H
125	0.267	0.266	0.483			H_2O		V.L.

[a] H = High; M = Medium; L = Low; V.L. = Very low.

using 147 planes was chosen for further discussion, due to simplicity. Although other runs gave higher resolution they did not alter conclusions based on 147 planes. Further details of the method are available [27].

The difference electron density map showed negative peaks for Fe(III) ions or distortions of zeolitic structure elements leading to gain in electron density, and positive peaks for Na(I) lost by ion-exchange or by displacement of other elements of zeolitic structure leading to a loss in electron density.

TABLE III. Ionic Radii (Å).

Co-ordination no. / Ion	2	4	6	8	12
O^{2-}	1.35	1.38	1.4		
Na^{+}			1.02	1.16	
Ca^{2+}			1 0	1.12	1.35
Cu^{2+}			0.73		
Fe^{3+} LS[a]			0.55		
Fe^{3+} HS[b]		0.49	0.65		
Si^{4+}		0.26	0.40		
Al^{3+}		0.39	0.53		

[a] LS = los spin. [b] HS = high spin.

Discussion

Identification of Fe(III) Peaks

Criteria used for identification of Fe(III) ions were:

a) Peak size

The scattering factor of an element depends on the number of electrons of the particular element. Since the atomic number of Fe(III) is 27 while that of Na is 11 it is expected that the peak size would be high for the Fe(III) elements when the loss of Na ions is random amongst the positions they occupy in the zeolitic structure.

b) Positions in the zeolites as given in the literature [19–26]

There are only a few sites available for the metal ions in the zeolitic structure of NaX. These sites are:

Site I in hexagonal prism (centre)

Site I′ opposite to Site I in truncated octahedron

Site II′ behind the hexagonal window inside the truncated octahedron

Site II opposite to Site II′ and in the supercage

Site III in front of tetragonal window of the truncated octahedron and inside the supercage

Site IV inside the supercage.

All these sites are lying on the diagonals of the cube of the unit cell, and the ions show preference for those sites as a result of coulombic forces and co-ordination preferences.

c) Interatomic distances and co-ordination spheres

Table III quotes the ionic radii of the elements of interest and their ionic radii in relation to their co-ordination number.

From Table III it is expected that if Fe(III) is in high spin state the distance between Fe(III) and zeolitic oxygen will be greater than 2.05 Å in octahedral co-ordination or greater than 1.9 Å in tetrahedral co-ordination.

According to Levina and Malashevitsh [28] the Fe(III) ion enters the zeolitic structure at pH = 4 as $Fe(OH)^{2+}$ and therefore it might be that one of the ligands is at a shorter distance than the others because it is an OH ion. However this does not seem to be justified from our analytical results which show a good balance between Fe(III) and Na(I) during ion exchange.

On the basis of the criteria stated previously, and on the assumption that the negative peaks arise from Fe(III) ions accompanied by their hydration sphere, the following negative peaks are assigned to Fe(III) ions in three alternative models.

Model 1

Peaks 2, 3, 4, 7, 14, 16, 109 represent Fe(III) ions. The NaX unit cell is comprised of eight truncated octahedra. A thirty percent exchanged sample (Fe(III) for Na(I)) would gain 9–10 Fe(III) and lose three times as many Na(I) ions per unit cell. In the case where no zeolitic structure breakdown is considered the possible Fe(III) sites are almost as numerous as the number of Fe(III) ions exchanged. It seems reasonable on that account to suggest that Fe(III) ions are randomly distributed in the different sites of the zeolitic structure thus showing no site selectivity in the hydrated form up to 30% exchange (Fig. 1, 2).

Apart from peak 109 all the other Fe(III) ions include water molecules in their co-ordination sphere. All sites show distorted octahedral co-ordination (the extent of distortion depending on the site) except for Site I′ which is compressed tetrahedral.

Model 2

Peaks 2, 3, near OW_3, 109 and 4 represent Fe(III) ions.

In this model minor distortions of the zeolitic framework are assumed to take place due to some displacement of the zeolitic oxygen under the influence of the Fe(III) positive charge during exchange. Evidence for distortions of zeolitic structure are the negative peaks obtained near zeolitic oxygens, the loss of Si or Al from the zeolitic structure positions and the gradual breakdown above 30%

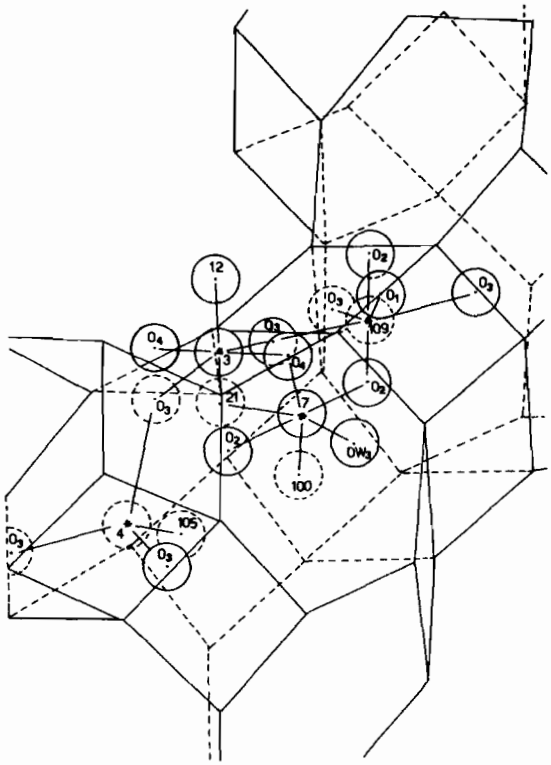

Fig. 1. Positions of some Fe(III) ion complexes in the zeolitic framework according to Model A. Fe(III) ions are marked with *.

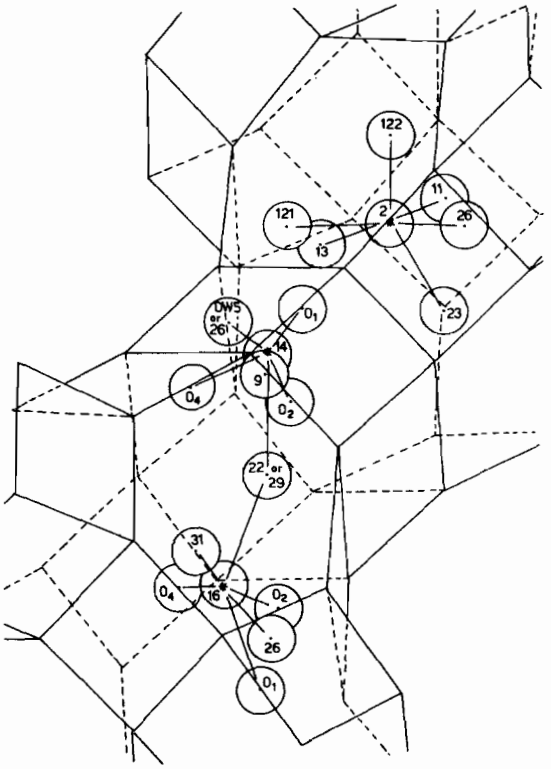

Fig. 2. Positions of some Fe(III) ion complexes in the zeolitic framework according to Model A. Fe(III) ions are marked with *.

exchange. This model presents distortions due to Fe(III) ions in hexagonal prisms (peak 109) (Fig. 15) and the Fe(III) ions in sites close to OW_3 in front of the hexagonal window (Fig. 3). This position on the map shows a positive peak. However because in this area the Site (II) of Na(I) exists and since the Na(I) loss is three times greater than the gain in Fe(III) it might be assumed that the Fe(III) ions accommodated in this position are considerably less than the sodium ions leaving this position during exchange and therefore the map shows a positive peak while the ligands of the Fe(III) ions are shown as negative peaks.

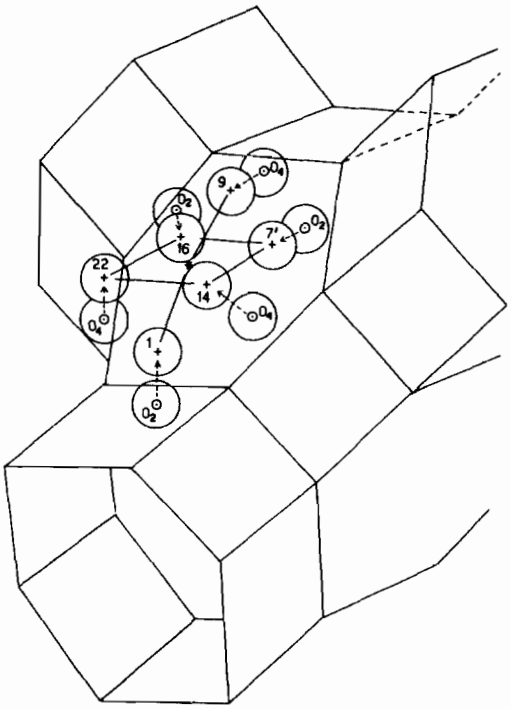

Fig. 3. Position of Fe(III) ion with co-ordinates (0.25, 0.0, 0.0) according to Model B.

Model 3

Peaks 2, 4 and 109 represent Fe(III) ions. This model supposes major distortions of the zeolite framework during exchange.

The distortions are mainly derived from displacements of Si or Al ions. This third model (Fig. 4, 5) based on major distortions of zeolitic structure is mainly the result of displacements of Si or Al ions from their original positions due to repulsion forces generated from Fe(III) ions entering the hexagonal prisms, where the Fe(III) is totally co-ordinated to zeolitic oxygens. These distortions give a locally amorphous appearance within the zeolitic structure although the basic structure as a whole still exists.

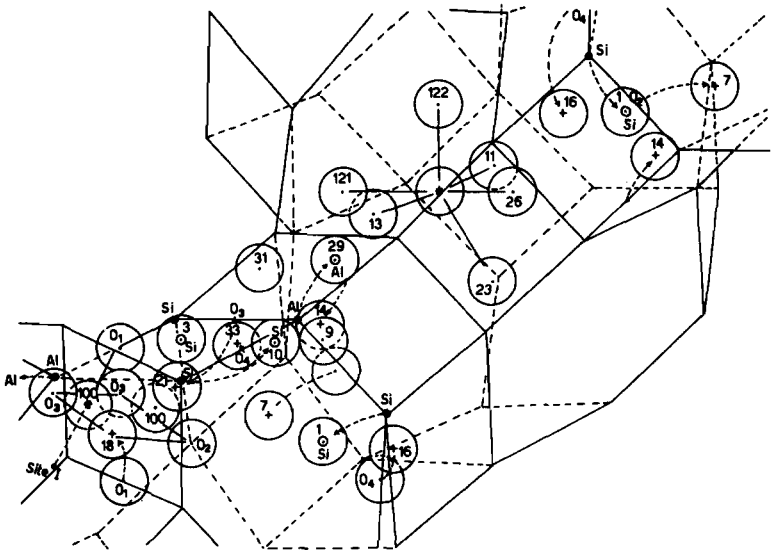

Fig. 4. A perspective view of Model C. Fe(III) are marked with asterisk.

Fig. 5. Model C. A perspective view of negative peaks in the supercage between two hexagonal windows of truncated octahedra.

Justification for this model is given from the loss of peak height in positions occupied by Si and Al ions in NaX crystal structure, in agreement with microporosity loss (8%) obtained from surface area measurements. Furthermore this model is consistent with the observed gradual breakdown at higher percentages of exchange.

Finally, Fig. 6–15 shows co-ordination schemes of Fe(III) ions in the zeolitic structure as they are found from the electron density map. Co-ordination schemes of Fig. 14 apply to Model 2 while Fig. 15 applies to Model 2 and Model 3.

From the difference electron density map it is fairly clear that during exchange with Fe(III) ion the pure exchange phenomenon is accompanied by changes in framework positions. There are peaks which can only be explained by minor displacements of oxygen ions of the zeolite framework and negative peaks which may be assigned to displacements of Si and Al ions.

These displacements of framework elements associated with exchange phenomena seem to provide the overall picture. Mechanistically, one can envisage exchange as first involving the simple replacement

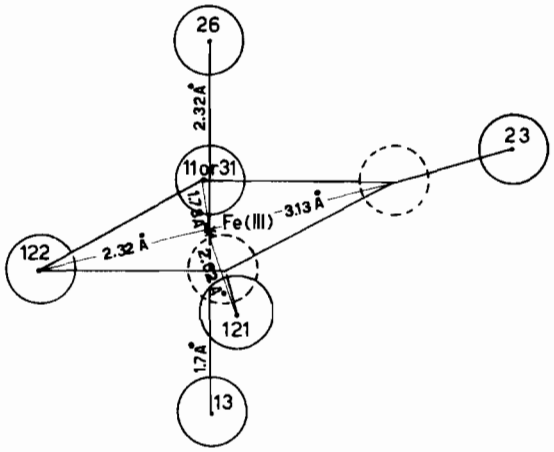

Fig. 6. Co-ordination scheme of Peak 2, for all models.

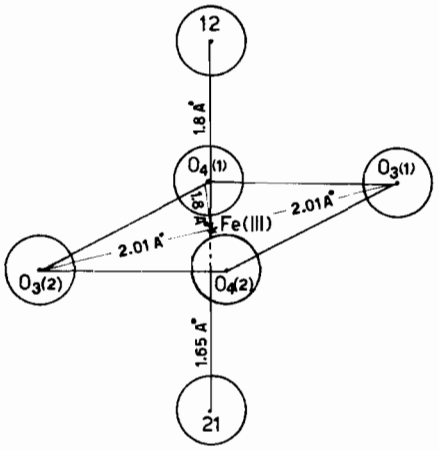

Fig. 7. Co-ordination scheme of Peak 3, for Models A, B.

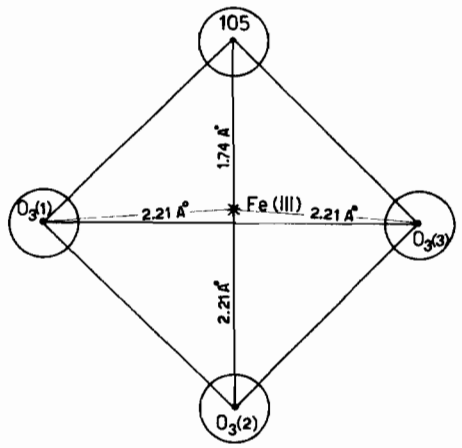

Fig. 8. Co-ordination scheme of Peak 4, for Models A, B, C.

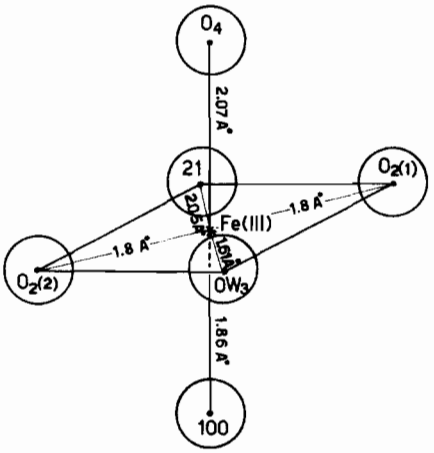

Fig. 9. Co-ordination scheme of Peak 7, for Model A.

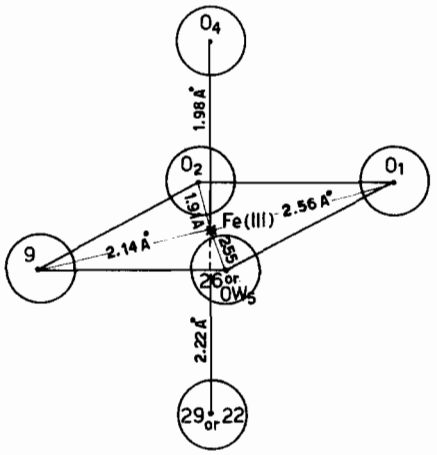

Fig. 10. Co-ordination scheme of Peak 14, for Model A.

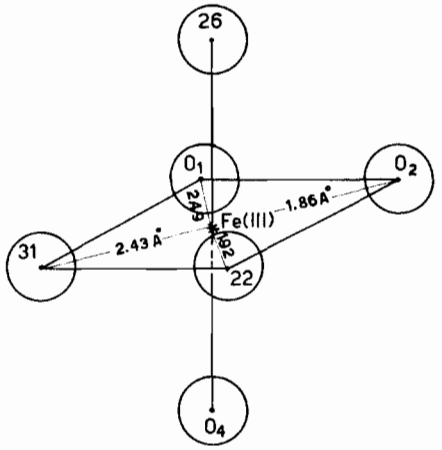

Fig. 11. Co-ordination scheme of Peak 16, for Model A.

of sodium by iron (not necessarily at the same sites) as typified by Model 1. As more iron enters and new co-ordination forces are set up, the framework distortions begin to occur as in Model 2. These distortions increase (with accompanying breakdown to amorphous material) as substantial percentages of iron are exchanged (Model 3).

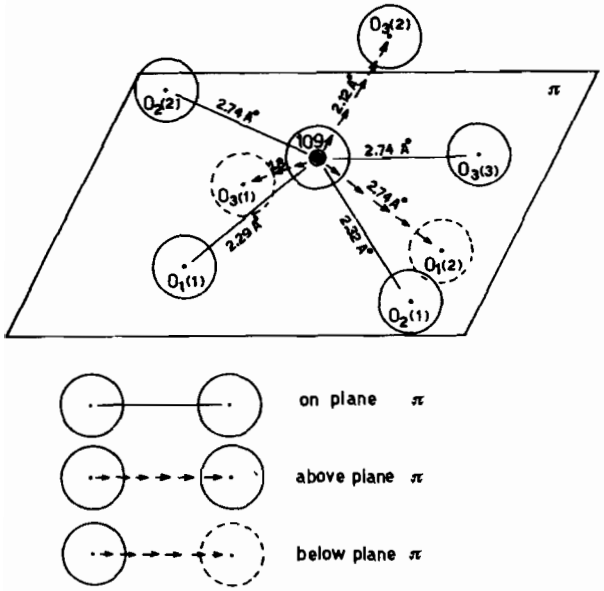

Fig. 12. Co-ordination scheme of Peak 109, for Model A.

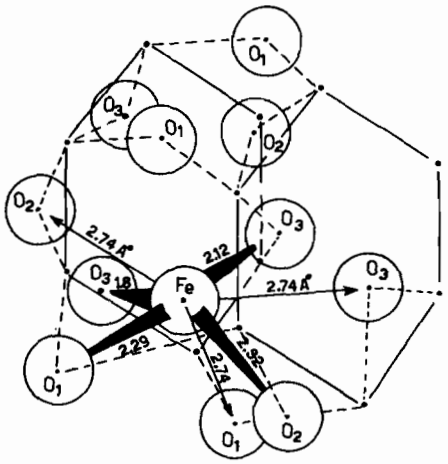

Fig. 13. Co-ordination scheme of Peak 109, for Model A.

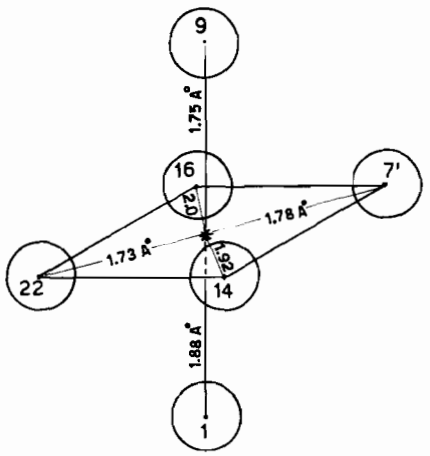

Fig. 14. Co-ordination scheme of Fe(III) at position (0.25, 0.0, 0.0) for Model B.

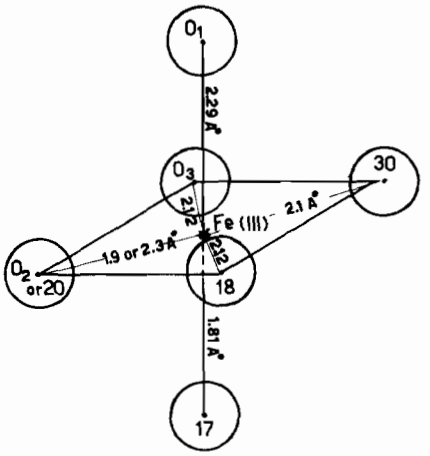

Fig. 15. Co-ordination scheme of Peak 109, for Models B and C.

Although, because of the above remarks, we tend to prefer Model 3 to describe the sample we studied, a conclusion has not definitely been established by the X-ray crystal structure analyses. It is necessary that further investigations (perhaps involving other techniques) be initiated to provide information for selecting between the options given here.

References

1 J. N. MacBain, "The sorption of gases and vapors by solids", Chapter 5, Rutledge (London), 1932.
2 R. M. Barrer, *Trans. Faraday Soc., 40,* 205 (1944).
3 R. M. Barrer, *Trans. Faraday Soc., 40,* 195 (1944).
4 R. M. Barrer, *Endeavour, 23,* 122 (1964).
5 R. H. Hilton, *U.S. Patents,* 2882243 and 2882244 (1959).
6 D. W. Breck, W. G. Eversole, R. M. Milton, T. B. Reed, and T. L. Thomas, *J. Am. Chem. Soc., 78,* 5963 (1956).
7 T. B. Reed and D. W. Breck, *J. Am. Chem. Soc., 78,* 5972 (1956).
8 O. Grubner, P. Jiru and M. Rolek, "Molecularslebe VEB Deutscher Verlag der Wissenschaften', Berlin, 1968.
9 J. A. Rabo, P. E. Pickert and R. L. Hays, *Ind. Eng. Chem., 53,* 733 (1961).
10 D. H. Stormont, *Oil Gas J., 62,* 52 (1964).
11 I. V. Scalkina, I. K. Kolchin, Ya. L. Margolis, N. F. Ermolenko and L. N. Malashevich, *Izv. Akad. Nauk SSSR, Ser. Khim., 5,* 929 (1970).
12 *Idem, Kinetika i Kataliz, 10,* 185 (1958).
13 *Idem, U.S.S.R. Patent* 239, 929 (1968). *Chem. Abs., 71,* 38311f (1971).
14 L. Eyres, *Ph.D. Thesis* UMIST (1972).
15 S. A. Levina, L. N. Malashevich, N. F. Ermolenko and A. A. Prokopovich, *Kolloidn. Zn., 24,* 828 (1967).
16 S. A. Levina, L. N. Malashevich and N. F. Ermolenko, *Dokl. Akad. Nauk Belorrussk SSR, 10,* 236 (1966).
17 M. A. Sidorovick, *Izv. Akad. Nauk Belorrussk SSR, Ser.* M. A. Sidorivick, *Izv. Akad. Nauk Belorrussk SSR, Ser. Khim. Nauk, No. 3,* 113 (1966).
18 S. A. Levina, L. N. Malashevich, N. F. Ermolenko, L. I. Piguzova and A. A. Prokopovich, *Izv. Akad. Nauk Belorrussk SSR, Ser. Khim. Nauk, No. 4,* ii (1966).

19 L. Broussard and D. P. Shoemaker, *J. Am. Chem. Soc., 88,* 1041 (1960).
20 F. D. Hunter and J. Scherzer, *J. Catalysis, 20,* 246 (1971).
21 P. Gallezot and B. Imelik, *J. Chem. Phys., 68,* 34 (1971).
22 P. Gallezot, Y. Ben Taarit and B. Imolik, *J. Catalysis, 26,* 295 (1972).
23 P. Gallezot and B. Imelik, *J. Phys. Chem., 77,* 652 (1973).
24 D. H. Olson, *J. Phys. Chem., 72,* 4366 (1968).
25 D. H. Olson, *J. Phys. Chem., 74,* 2758 (1970).
26 I. E. Maxwell and J. J. De Boer, *Chem. Comm.* (1974).
27 N. P. Evmerides, *Ph.D. Thesis, Vol. 1,* UMIST (1976)
28 L. N. Malashevich, S. A. Levina and N. F. Ermolenko, *Kolloidnyi Zn., 31,* 543 (1969).